J Porous Mater (2017) 24:1647–1654
DOI 10.1007/s10934-017-0404-3

Effect of modification on Pd dispersion, acidity, sulfur resistance and catalysis of Pd/Al-MCM-41 zeolite

Ruizhi Chu[1,2] · Wenxin Hou[1] · Tingting Xu[1] · Xianliang Meng[1,2] · Zhenyong Miao[1] · Songpeng Cheng[1]

Published online: 16 March 2017

Abstract A series of Pd catalysts supported on modified Al-MCM-41 zeolite were prepared by impregnation and dimethyl ether synthesis from sulfur-containing syngas over hybrid catalysts. The effect of acid or acid/M_xO_y (CeO_2, ZnO or ZrO_2) on the Pd dispersion, acidity, sulfur-resistance and catalysis of a Pd/Al-MCM-41 zeolite was investigated. Acid-modified Pd/Al-MCM-41 zeolite effectively increased the number of moderate acidic sites. However, the Al-MCM-41 zeolite was collapsed due to destruction of the acid on the structure, which decreased the active surface area of the Pd phases. Adding M_xO_y effectively fixed SO_4^{2-}, reduced destruction of the catalyst structure and stabilized the effect of acid on the acidity. In addition, the M_xO_y fixed SO_4^{2-} effectively, which reduced SO_4^{2-} by reacting with the overflow hydrogen to generate H_2S, thus stabilizing the catalytic activity of Pd. It was found that Pd supported on 0.4 mol L^{-1} H_2SO_4/1% ZrO_2 modified the stable Al-MCM-41 zeolite and showed excellent CO conversion and DME selectivity as well as high stability in sulfur-containing syngas. CO conversion and DME selectivity were 66.5 and 64.0%, respectively, after a 20 h stream was applied at a sulfur-containing syngas, with a pressure of 3 MPa, temperature of 300 °C and space velocity of 1600 L kg^{-1} h^{-1}.

✉ Xianliang Meng
hwxcumt@163.com

[1] Key Laboratory of Coal-based CO2 Capture and Geological Storage, Jiangsu Province (China University of Mining and Technology), Xuzhou 221116, China

[2] School of Chemical Engineering and Technology, China University of Mining and Technology, Xuzhou 221116, China

Keywords Modification · Pd/Al-MCM-41 catalyst · Sulfur-resistance · Acidity · Dimethyl ether · Pd dispersion

1 Introduction

Mesoporous MCM-41 zeolite belongs to a group of materials with great potential for catalysis applications due to their unique properties, such as a uniform porous structure, large surface area and high porosity [1]. However, the acidity of MCM-41 is weak, and this material exhibits low catalytic activity in reactions that employ strong and moderate acid catalysts [2–4]. Recent studies show that a modified Al-MCM-41 zeolite with moderate acidity and mesopore structure may be promising for catalytic reactions [3, 5, 6]. At present, Al-MCM-4l has been used as an effective catalyst for the reaction of pyrolysis [7–9], hydrogenation [10, 11], isomerization and alkylation [12, 13]. However, the acidity and thermal stability of Al-MCM-41 is still lower than that of the commonly used ZSM-5 and HY catalysts [3], which has prompted researchers to work on improving them. Previous researches show that acid-modified [14, 15] and oxide-modified [16–18] zeolite exhibit special acidic properties. In particular, CeO_2 [19, 20], ZnO [21] and ZrO_2 [22, 23] as common catalyst promoter are added to zeolite, which firm structure and adjust surface acidity of zeolite catalyst. In our previous research, a series of ZSM-5 [24] and γ-Al_2O_3 [25, 26] hybrid catalysts with different promoters were prepared by impregnation, and found these promoters can improve catalyst activity and stability.

At present, bifunctional catalysts were used in syngas-to-dimethyl ether (STD), which was formed by combining two catalysts: the metal catalyst for synthesizing methanol and the solid acid catalyst for methanol dehydration to DME [27]. Moderate acidity and sulfur

tolerance of the catalyst is important. Researchers often choose a highly specific, mesoporous metal catalyst with a large surface area and a high content moderate acid as the solid acid catalyst, which improves the selectivity of DME [28–30].

Our research group [31] found that the loaded noble metal Pd on a solid acid carrier displayed enhanced activity in the synthesis of methanol by improving the sulfur tolerance of the catalyst. Pd catalysts exhibit resistance to sintering and sulfur poisoning, which can slow down the effect of high temperature deactivation and sulfur poisoning on the catalyst. Our research group [32] also found the types of carriers and modifiers that influence the activity of the catalyst and selectivity of the reaction.

Therefore, in this paper, we chose Pd/Al-MCM-41 as the catalyst for the STD reaction and studied the influence of acid or acid/M_xO_y (CeO_2, ZnO or ZrO_2) as modifiers of Al-MCM-41 zeolite on the pore diameter distribution, Pd dispersion, surface acidity, skeleton construction and catalysis of Al-MCM-41 zeolite. The interaction between the Pd active surface, acid surface and modifiers was used to explain the improved catalytic performance.

2 Experimental

2.1 Treatment procedure of Al-MCM-41

2.1.1 Acid treatment

Five grams of Al-MCM-41 (particle size 0.6–0.9 mm) was impregnated with acid solution in a 150 mL flask at 50 °C for 2 h. The suspension was then evaporated under 80 °C followed by a 560 W microwave incubation for 1 h to obtain the following acid modified samples: XHBO, XHPO and XHSO (where X is the concentration of the acid in mol L^{-1}; HBO, HPO and HSO are H_3BO_3, H_3PO_4, and H_2SO_4, respectively).

2.1.2 Acid/M_xO_y treatment

Metal oxide (M_xO_y) was loaded on 5 g of Al-MCM-41 in a metal solution ($Ce(NO_3)_3$, $Zr(NO_3)_4$ or $Zn(NO_3)_2$) under the same preparation conditions. Then M_xO_y treated Al-MCM-41 catalysts were modified with SO_4^{2-} using the same process as described previously to obtain the acid/M_xO_y treated Al-MCM-41 catalysts. The H_2SO_4 concentration for these catalysts was 0.4 mol L^{-1}, and the composite modifiers were marked as SO_4^{2-}/z% M_xO_y (where z% represents the load of M_xO_y, g/g Al-MCM-41).

2.2 Catalyst preparation

Pd was loaded on 5 g of acid- or acid/M_xO_y-treated Al-MCM-41 in a 0.02 mol L^{-1} $PdCl_2$ solution under the same preparation conditions. The load of Pd was 2% (g Pd/ g Al-MCM-41).

2.3 Characterization

The surface area, pore size, and pore volume were determined from nitrogen adsorption/desorption isotherms at −196 °C, using a fully automated AS1V150 gas adsorption device. Before analysis, all the samples were outgassed at 150 °C under vacuum for 2 h. The specific surface area was calculated from adsorption curve according to the Brunauer–Emmet–Teller (BET) method. Pore size and pore volume of micropores and mesopores are calculated according to the Horwarth–Kavazoe (HK) and Barrett–Joyner–Halenda (BJH) methods respectively. The pore size distributions are calculated using the regularization method according to the density functional theory (DFT), based on a molecular model of nitrogen adsorption in porous solids.

X-ray Diffraction (XRD) patterns measurements were recorded on a diffraction instrument (D/Max-3B, 35 kV, 30 mA) using a Cu-Kα X-ray source in the range of $2\theta = 1.4\text{-}8.0°$.

CO-temperature-programed desorption (CO-TPD) measurements were performed in a continuous-flow apparatus using a linear quartz micro-reactor (d_{int}, 4 mm) with ca. 15 mg of catalyst. The CO-TPD experiment was carried out in the range of 25–554 °C at a heating rate of 20 °C min^{-1} with CO flowing at 60 STP mL min^{-1}. The desorbed CO was monitored by a gas chromatograph with a TCD detector. Before recording measurements, the samples were treated at 500 °C for 30 min under nitrogen flow. The stoichiometric coefficient of chemisorption was calculated according to CO/Pd = 1.

Ammonia temperature-programed desorption (NH_3-TPD) measurements were also performed in a continuous-flow apparatus using a linear quartz micro reactor (d_{int}, 4 mm) loaded with ca. 15 mg of catalyst. The NH_3-TPD experiment was carried out in the range of 25–650 °C at a heating rate of 20 °C min^{-1} with NH_3 flowing at 60 STP mL min^{-1}. The desorbed ammonia was monitored by a gas chromatograph with a TCD detector. Before recording measurements, the samples were treated at 500 °C for 30 min under nitrogen flow.

Fourier transform infrared (FT-IR) spectra were recorded in the range of 400–4000 wave number (cm^{-1}) at room temperature. All samples were prepared as KBr pellets and analyzed on a NICOLET 380 FTIR spectrometer.

The sulfur content of the sample was determined using a YX-DL/Q-type sulfur meter (Youxin Instrument Manufacturing Co., Ltd.). The sample (0.05 g) was weighed in a porcelain dish and then covered with a thin layer of WO_3. After delivering the sample to the device, a coulomb titration procedure was performed prior to obtaining the mass percentage data.

2.4 Catalyst evaluation

The synthesis of DME from syngas was carried out in the gas phase in a WSFM pressurized fixed-bed microreactor, using a reaction tube with a 5 mm inner diameter. Approximately 0.5 g of the catalyst was loaded into the tube and placed between two quartz wool plugs. The catalyst was heated to 220 °C under a 1 °C min^{-1} hydrogen flow and maintained at temperature for 2 h. Then, H_2, CO, N_2, CO_2, H_2S and thiophene (volume ratio H_2:CO:N_2:CO_2:H_2S:thiophene = 50:25:19:5:0.5:0.5, and space velocity 1600 L kg^{-1} h^{-1}) were introduced through a mass flow controller, slow step-up to pressure 3 MPa, temperature 300 °C to initiate the reaction. The reaction products vent through the exhaust valve after decompression, which enables chromatographic analysis.

3 Results and discussion

3.1 Modification with acid

The pore size distribution of the Pd/Al-MCM-41 catalysts was changed from single to double after acid treatment, and the pore size distribution of H_2SO_4-modified samples was relatively concentrated (Fig. 1a). The specific surface area and pore volume of the samples decreased significantly after acid modification (Table 1). The mesoporous size increases when the H_2SO_4 concentration increases, whereas the specific surface area and mesoporous volume decrease (Table 1). These results show that the hydrothermal stability of Pd/Al-MCM-41 samples decreased after acid modification. This may be due to the acid radical destroying the structure or perhaps the H^+ participating in the hydrothermal reaction, which causes the pore structure of the Pd/Al-MCM-41 samples to collapse. The Pd dispersion of the samples decreases with the acid treatment, while the PdO

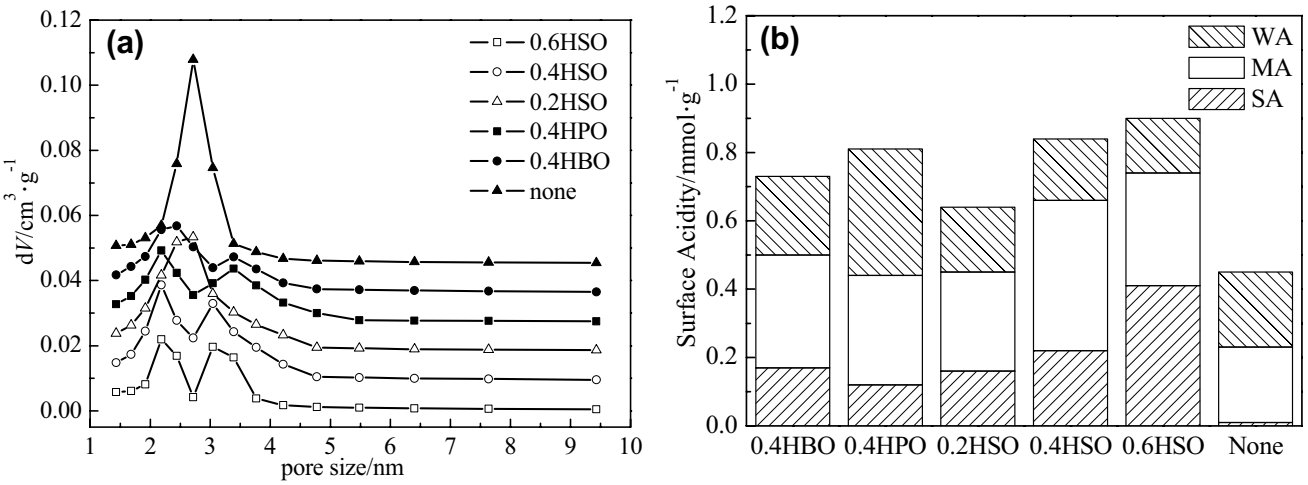

Fig. 1 Pore size distribution (**a**) and surface acidity (**b**) of acid-modified catalysts

Table 1 Pd dispersion, PdO size, texture and phase structure properties of acid-modified catalysts

Samples	Pd dispersion (%)	PdO size (nm)	Surface area (m^2 g^{-1})	Pore size /nm	Pore volume (cm^3 g^{-1})
0.4HBO	16.51	6.66	554.7	3.1	0.6199
0.4HPO	13.35	8.24	458.2	3.3	0.5268
0.2HSO	17.26	6.37	634.2	2.9	0.7046
0.4HSO	16.63	6.61	587.3	3.2	0.6541
0.6HSO	14.99	7.34	433.5	3.7	0.4983
None	25.95	4.24	757.6	2.8	0.9317

grain size increases (Table 1). Therefore, acid modification reduces the active surface area of the Pd metal on the surface of the Al-MCM-41 zeolites, in addition to pore structure collapse and a decrease in the specific surface area.

The active site of the methanol dehydration reaction in STD is moderate acid [30, 33]. The number of weak acid sites has little effect on the selectivity of DME. Strong acid sites are hydrocarbon by-product generation centers, which trigger DME decomposition reactions. Acid modification can effectively increase the surface acidity of Pd/Al-MCM-41 (Fig. 1b). As a result, the surface acidity of the acid modified catalysts substantially increases compared to the unmodified versions of these catalysts at the same acid concentration, with maximum total acidity achieved after modifying Pd/Al-MCM-41 with H_2SO_4. The total surface acidity for a catalyst with strong acidity increases due to the increase in H_2SO_4 concentration, while the surface acidity for catalysts with moderate acidity increases initially and then decreases. Although acid modification results in structural collapse and a decrease in the specific surface area, the surface acidity is effectively improved, especially under moderately acidic reaction conditions. The effects of moderate acidity are most pronounced in 0.4 mol L^{-1} H_2SO_4, when the Pd dispersion is 16.63%, specific surface area is 587.3 m^2 g^{-1}, and pore volume is 0.6541 cm^3 g^{-1}.

3.2 Modification with SO_4^{2-}/M_xO_y

To further adjust the surface structure and acidity of the catalysts, the Pd/Al-MCM-41 catalysts were modified with SO_4^{2-}/M_xO_y in 0.4 mol L^{-1} H_2SO_4.

The specific surface area and pore volume of the samples increased after adding the metal oxides (Table 2). This may be because the SO_4^{2-}/M_xO_y forms a fixed SO_4^{2-} structure, which causes the interaction between M_xO_y and SO_4^{2-} to inhibit the destruction of SO_4^{2-} on the structure of the Pd/Al-MCM-41 and improve the stability of the structure. When the additive amount of ZrO_2 is less than 1%, the interaction between SO_4^{2-} and ZrO_2 increases with the increased ZrO_2 load. This enhances the damaging effects of SO_4^{2-} that weaken the Al-MCM-41 structure, which subsequently increases the specific surface area of the samples. When the additive amount of ZrO_2 is greater than 1%, the specific surface area of the samples decreases in response to the increased ZrO_2 load, perhaps due to excessive ZrO_2 aggregation on the surface of Al-MCM-41, resulting in partial channel blockage. In addition, the size of PdO grains on the sample surface decreases to varying degrees, which caused the Pd dispersion to increase after adding M_xO_y. These observations further indicate that adding M_xO_y inhibits the damaging effects of SO_4^{2-} on the structure of Al-MCM-41, which prevents the Pd grains from being embedding on the surface and increases the active surface area accordingly.

The research literature [28, 34, 35] confirms that the characteristic absorption peaks of Al-MCM-41 zeolites are located at 1089, 790 and 460 cm^{-1}, where the broad band at 1089 cm^{-1} and the band at 790 cm^{-1} correspond to the asymmetric and symmetric Si-O or Al-O stretching vibrations, and the band at 460 cm^{-1} indicates the bending vibrations of surface Si-O groups. In addition, all the samples exhibit an HSO_4^- stretching vibration absorption peak at 543 cm^{-1} [36, 37] and a weak characteristic absorption peak for S=O at 1382 cm^{-1} in addition to the Al-MCM-41 sample [37, 38], suggesting that the sulfate group has been successfully anchored on the walls of Al-MCM-41.

The addition of ZrO_2 and CeO_2 significantly enhances the characteristic peak at 3132 cm^{-1}, which appears as a Si–O–H stretching vibration peak at 960 cm^{-1} (Fig. 2a) [39, 40]. This indicates that adding CeO_2 and ZrO_2 enhances the binding capacity between the Al-MCM-41 surface and water under the same conditions. This may be due to the d space orbit of Ce and Zr combined with water, leading to enhanced absorption of the hydroxyl, which confirms that the addition of CeO_2 and ZrO_2 can effectively adjust the surface acidity of Al-MCM-41. In addition, the absorption peak of SO_4^{2-}/1% ZrO_2 at 1089 cm^{-1} is red shifted compared to the low-wavenumber Al-MCM-41. In general, a greater than 2 cm^{-1} red shift of this peak is considered evidence of metal loading onto the Al-MCM-41 skeleton [41]. The addition of CeO_2 and ZnO to the samples does not appear to cause a red shift. This proves that other metals added to the sample do not enter into the Al-MCM-41 skeleton. This phenomenon will likely affect the catalytic performance of the sample.

The Si-O-Si absorption peak of the SO_4^{2-}/1% ZrO_2 modified sample is shifted from 1089 to 1080 cm^{-1}, with the red shift amplitude reaching 9 cm^{-1} compared to the Al-MCM-41 sample (Fig. 2b). The amount of Zr^{4+} entering the Al-MCM-41 skeleton increases with the increase in ZrO_2 load when the quantity is less than 1%, which aggravates the impact on the zeolite framework. When the ZrO_2 load quantity is more than 1%, the Zr^{4+} saturates the framework. Therefore, when the ZrO_2 load further increases, the excess ZrO_2 only crystallizes on the Al-MCM-41 surface during the baking process, so the skeleton structure does not change. In addition, the absorption peak intensity of Si-O-Si at 1089 cm^{-1} increased initially and then decreased. This may be due to the Zr^{4+} in the zeolite framework enhancing the vibration strength of samples with a low ZrO_2 load. When the ZrO_2 load is high, the strong interaction between the ZrO_2 crystal grains and the Zr^{4+} in the zeolite framework weakens the asymmetric stretching vibration of Si–O–Si. Consequently, the absorption peak of 1120–1220 cm^{-1} enhances when adding ZrO_2 (Fig. 2b). A

Table 2 Pd dispersion, PdO size, texture and phase structure properties of SO_4^{2-}/M_xO_y-modified catalysts

Samples	Pd dispersion (%)	PdO size (nm)	Surface area ($m^2\ g^{-1}$)	Pore Size /nm	Pore volume ($cm^3\ g^{-1}$)
SO_4^{2-}/1% CeO_2	25.44	4.32	713.6	2.9	0.8045
SO_4^{2-}/1% ZnO	20.34	5.41	708.5	2.9	0.7878
SO_4^{2-}/1% ZrO_2	25.24	4.36	689.3	3.0	0.7311
SO_4^{2-}/0.5% ZrO_2	21.56	5.10	616.8	3.1	0.6842
SO_4^{2-}/2% ZrO_2	24.90	4.42	653.2	3.0	0.7182
SO_4^{2-}/3% ZrO_2	25.02	4.40	616.4	3.0	0.6911
0.4HSO	16.63	6.61	587.3	3.2	0.6541

band at 1120 and a band at 1198 cm^{-1} relate to ligand of high valence sulfur and metal oxides [42].

The CO bridge species of the samples shift to a lower desorption temperature zone after adding M_xO_y (Fig. 3a). This shows that the adsorption ability of the catalyst on CO becomes weak with the addition of oxides. The decrease in the desorption temperature for the ZrO_2 samples is the largest at 70 °C. This may be the impact Zr^{4+} conveys on the Al-MCM-41 skeleton structure. The addition of CeO_2 significantly enhances the bridge adsorption capacity of CO, but the CO desorption temperature changes slightly. The addition of ZnO widens the range of possible CO desorption temperatures, which means the size distribution of the Pd grains increases while the evenness decreases. This leads to deactivation of the catalysts during the reaction. When the addition amount of ZrO_2 is below 2%, the CO adsorption capacity decreases slightly with increased addition of ZrO_2 and influences the CO desorption temperature range (Fig. 3b). When the ZrO_2 addition amount is 1%, the width of the desorption peak is narrowest. When the ZrO_2 addition amount is 3%, the CO desorption temperature increases to a higher temperature zone.

The addition of M_xO_y can significantly change the surface acidity of Pd/Al-MCM-41 catalyst distribution (Figs. 1b, 4). Under the same conditions, moderate acid and strong acid increased largest in adding ZrO_2 samples. With larger addition amounts of ZrO_2, the total surface acidity of strong acid samples increases rapidly, while the total surface acidity of moderate acid samples reduces accordingly. When the added amount of ZrO_2 is 1%, the total acidity reaches a maximum.

3.3 Evaluation of the sulfur-resistance and stability of the catalyst

Excellent catalytic performance is evaluated based on whether a catalyst maintains good catalytic activity under long reaction time conditions, but many catalysts tend to exhibit a decline in catalytic performance after a relatively short period of time for various reasons. Stability tests of Pd/Al-MCM-41 (PM), SO_4^{2-}/Pd/Al-MCM-41 (SPM), SO_4^{2-}/ZrO_2/Pd/Al-MCM-41 (SZPM) and Cu/ZnO/Al_2O_3 + HZSM-5 (CZA) in STD reactions were carried out for 20 h, in which the referenced CZA catalysts were used.

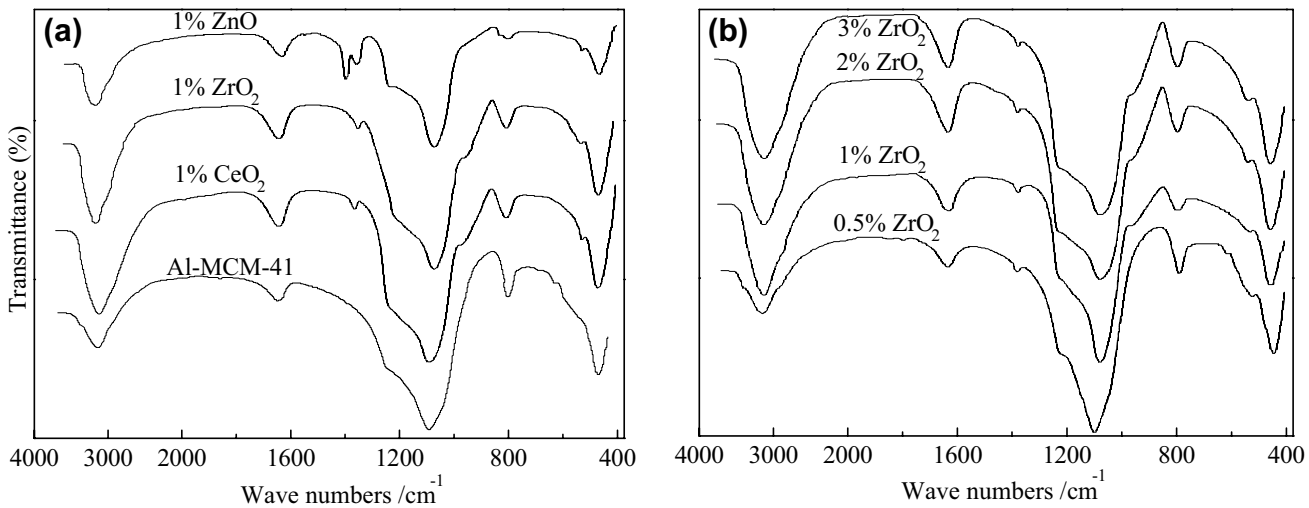

Fig. 2 IR spectra of SO_4^{2-}/M_xO_y-modified catalysts

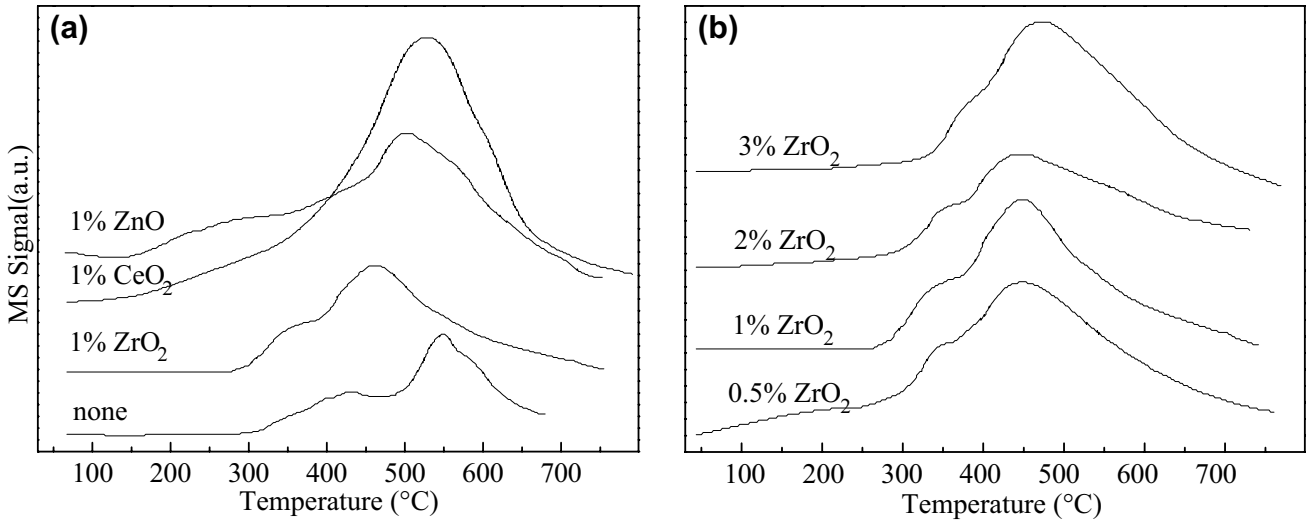

Fig. 3 CO-TPD of SO_4^{2-}/M_xO_y-modified catalysts

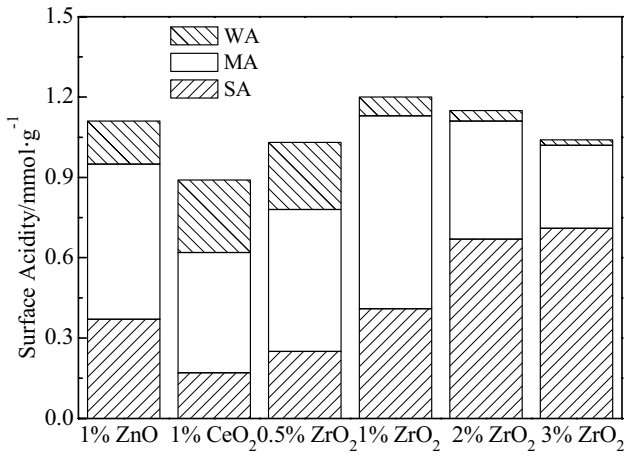

Fig. 4 Surface acidity of SO_4^{2-}/M_xO_y-modified catalysts

The PM catalyst maintains good STD reaction stability within 3 h. After 20 h, the catalyst quickly loses activity, and the conversion rate of CO is reduced to 35.5%. The SPM catalyst quickly loses activity at the beginning of the reaction and the CO conversion is reduced from 61.2 to 55.1% within 20 h of the STD reaction. The SZPM catalyst reacts for 5 h at 300 °C, but the conversion of CO decreases from 69.4 to 66.5% by 20 h, and no further inactivation is observed (Fig. 5a). The selectivity of the CZA and SZPM catalysts to DME decreases slightly during the 5 h reaction time, and the selectivity of the SPM catalyst to DME initially increases rapidly but then rapidly declines (Fig. 5b). The selectivity of the SZPM catalyst to DME always maintains more than 64.0% within 20 h of initiating the STD reaction, which is significantly higher than that of the PM and SPM catalysts. These results indicate that the catalytic stability of the SZPM catalyst is better than that of the PM, SPM and common CZA catalysts. This indicates that sulfate modified Pd/Al-MCM-41 does increase the amount of moderate acid and that adding ZrO_2 effectively stabilizes the surface active acid sites and the active Pd to improve the catalytic performance of the SZPM catalyst. Another factor may be the hydrophilic ZrO_2, which can quickly transfer the water adsorbed on the Al-MCM-41 surface to maintain the active sites that participate in the STD reaction.

The specific surface area, pore volume and Pd dispersion of each sample decrease to different degrees after the reaction (Table 3). The parameters of the SZPM catalyst decrease the least, whereas the Pd dispersion only decreases by 1.52%. As stated previously, acid modification results in structural collapse and a decrease in the specific surface area. Table 3 shows that the addition of ZrO_2 improves the stability of the catalyst, including the catalyst structure and Pd dispersion, which effectively explains the results of the catalytic stability tests shown in Fig. 5. In addition, the sulfur content decrease of the SZPM catalyst is substantially less than that of the SPM catalyst after a 20 h reaction. This result also supports the explanation presented in "Modification with acid" section that the metal oxide and SO_4^{2-} form a fixed SO_4^{2-} structure, which reduces the loss of SO_4^{2-}.

Small-angle XRD spectrum of the SZPM-fresh and SZPM-used was shown in Fig. 6a, three distinct diffraction peaks (100), (110) and (200) could be readily indexed to MCM-41 [43]. In addition, it also indicated the sample structure unchanged after stability testing. The surface acidity of each sample reduces to varying degrees following the reaction, in which the parameter reduction of the SZPM catalyst is only 7.5% (Fig. 6b). This demonstrates

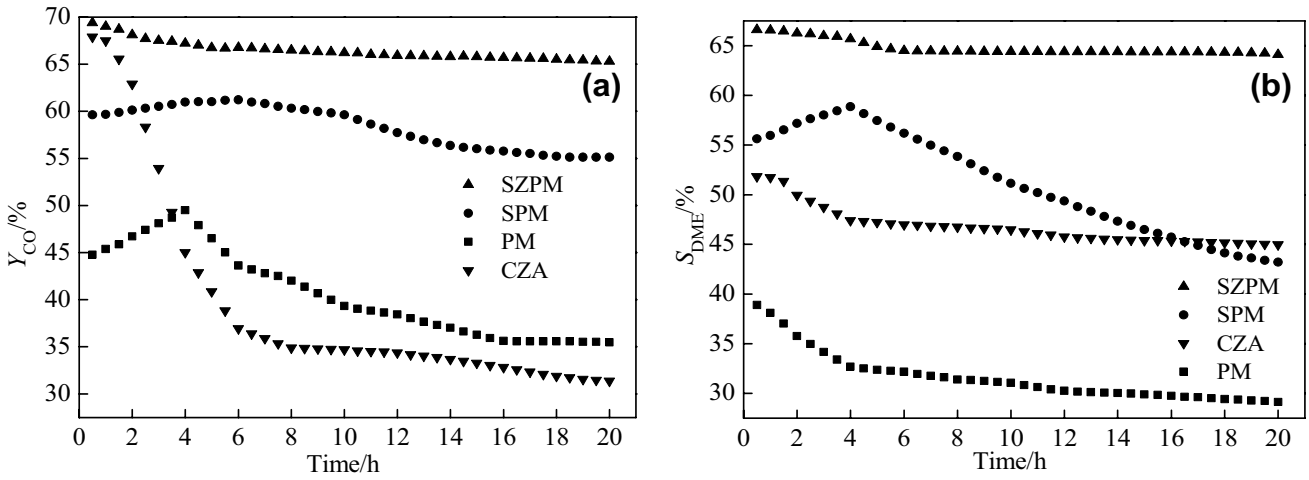

Fig. 5 CO conversion (**a**) and DME selectivity (**b**) of catalysts in STD reactions

Table 3 Surface areas, pore volumes and Pd dispersion of catalysts after stability testing

Catalysts	Surface area ($m^2\ g^{-1}$)	Pore volume ($cm^3\ g^{-1}$)	Pd dispersion (%)	Sulfur content (%)
PM				
Fresh	757.6	0.9317	25.95	–
Used	566.4	0.6308	11.36	–
SPM				
Fresh	587.3	0.6541	16.63	0.348
Used	564.5	0.6225	10.38	0.175
SZPM				
Fresh	689.3	0.7878	25.24	0.302
Used	673.1	0.7546	23.72	0.287

that the surface acidity of the SZPM catalyst exhibits the best stability under these reaction conditions. As mentioned earlier, SO_4^{2-} is very unstable when added alone. This is likely because SO_4^{2-} easily reacts with the overflow hydrogen to generate H_2S, which causes the irreversible loss of SO_4^{2-} and reduces the surface acidity of catalyst. In addition, the generated H_2S is likely adsorbed by Pd, further causing Pd sulfur poisoning, which leads to a reduction in methanol synthesis activity sites. Previous experiments have demonstrated that part of the SO_4^{2-}/ZrO_2 complex formed a fixed SO_4^{2-} structure, which decreased the amount of H_2S generated. Therefore, the active Pd and the surface active acid sites could be better stabilized. These results also explain the test results in Fig. 5 and Table 3.

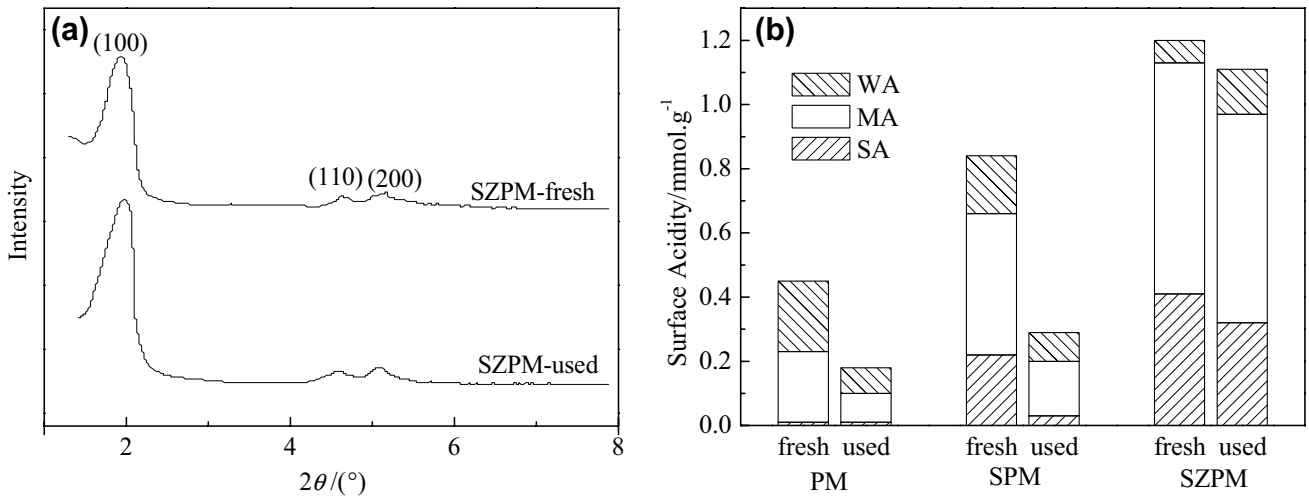

Fig. 6 Small-angle XRD spectrum of the SZPM-fresh and SZPM-used (**a**) and surface acidity of catalysts after stability testing (**b**)

4 Conclusions

In this study, Pd/Al-CMC-41 catalysts were modified by acids or by acids and metal oxides combined. The weak acidity and poor thermal stability of Pd/Al-MCM-41 in water contributes to its poor performance in methanol dehydration reactions. Acid modification adjusts the surface acidity of the Pd/Al-MCM-41 catalyst, but this makes the pore structure collapse and the specific surface area decrease. Moderate acidity samples displayed the most comprehensive results for Pd dispersion, specific surface area and pore volume when modified in 0.4 mol L^{-1} H_2SO_4. Adding M_xO_y effectively fixes SO_4^{2-} and reduces the generated H_2S, which stabilizes the surface active acid sites and the active Pd. Comprehensive analysis of the characterization parameters of Pd/Al-MCM-41 when modified with SO_4^{2-}/M_xO_y indicates that 1% ZrO_2 yielded the best results. The CO conversion and DME selectivity of the SO_4^{2-}/ZrO_2-modified catalyst in the STD reaction greatly improve, retaining 66.5% and 64.0% selectivity, respectively, over the course of a 20-h STD reaction.

Acknowledgements This work is supported by the Fundamental Research Funds for the Central Universities (2017XKQY067).

References

1. S.T. Wong, J.F. Lee, J.M. Chen, C.Y. Mou, J. Mol. Catal. A **165**, 159 (2001)
2. A. Ghanbari-Siahkali, A. Philippou, J. Dwyer, M.W. Anderson, Appl. Catal. A 192, 57 (2000)
3. K.Y. Kwak, M.S. Kim, D.W. Lee, Y.H. Cho, J. Han, T.S. Kwon, K.Y. Lee, Fuel **137**, 230 (2014)
4. T. Ehiro, A. Itagaki, H. Misu, K. Nakagawa, M. Katoh, Y. Katou, W. Ninomiya, S. Sugiyama, J. Chem. Eng. Jpn. **49**, 152 (2016)
5. E.G. Vaschetto, G.A. Monti, E.R. Herrero, S.G. Casuscelli, G.A. Eimer, Appl. Catal. A **453**, 391 (2013)
6. X.F. Zhang, F. Liu, X. Yang, J. Porous. Mater **23**, 1255 (2016)
7. F. Yu, L. Gao, W. Wang, G. Zhang, J. Ji, J. Anal. Appl. Pyrolysis **104**, 325 (2013)
8. K.K.V. Castro, A.A.D. Paulino, E.F.B. Silva, T. Chellappa, M.B.D. Lago, V.J. Fernandes, A.S. Araujo, J. Therm. Anal. Calorim. **106**, 759 (2011)
9. A.I. Casoni, M.L. Nievas, E.L. Moyano, M. Álvarez, A. Diez, M. Dennehy, M.A. Volpe, Appl. Catal. A **514**, 235 (2016)
10. M. Luo, Q. Wang, G. Li, X. Zhang, L. Wang, L. Han, Catal. Lett. **35**, 6 (2013)
11. R. Nares, J. Ramírez, A. Gutiérrezalejandre, R. Cuevas, Ind. Eng. Chem. Res. **48**, 1154 (2009)
12. J.J. Zou, N. Chang, X. Zhang, L. Wang, Chemcatchem. 4, 1289 (2012)
13. J.R. Sirkin, Chin, J. Catal. **31**, 759 (2010)
14. P. Monash, G. Pugazhenthi, Adsorption **15**, 390 (2009)
15. G. Dobele, T. Dizhbite, M.V. Gil, A. Volperts, T.A. Centeno, Biomass Bioenergy **46**, 145 (2012)
16. S. Ajaikumar, A. Pandurangan, Appl. Catal. A **357**, 184 (2009)
17. G.S.P. Soylu, Z. Özçelik, İ. Boz, Chem. Eng. J. **162**, 380 (2010)
18. H.G. Liao, D.H. Ouyang, J. Zhang, Y.J. Xiao, P.L. Liu, F. Hao, K.Y. You, H.A. Luo, Chem. Eng. J. **243**, 207 (2014)
19. A. Mates, Int. Nano Lett. **2**, 1 (2012)
20. J.P. Kumar, P.V.R.K. Ramacharyulu, G.K. Prasad, A.R. Srivastava, B. Singh, J. Porous Mater. **22**, 91 (2015)
21. T. Gong, L. Qin, J. Lu, H. Feng, Phys. Chem. Chem. Phys. **18**, 601 (2015)
22. L.J. Gao, Q.Q. Shang, J.J. Zhou, G.M. Xiao, R.P. Wei, Asian J. Chem. **25**, 6579 (2013)
23. F.B. Derekaya, G. Yaşar, Catal. Commun. **13**, 73 (2011)
24. R.Z. Chu, W.X. Hou, X.L. Meng, T.T. Xu, Z.Y. Miao, G.G. Wu, L. Bai, Chin. J. Chem. Eng **24**, 1735 (2016)
25. R.Z. Chu, T.T. Xu, X.L. Meng, G.G. Wu, W.X. Hou, Chem. Ind. Eng. Prog. **35**, 2474 (2016)
26. X.L. Meng, R.Z. Chu, B. Qin, E.W. Yue, T.T. Chen, X.Y. Wei, Energy Source Part A **37**, 870 (2015)
27. J.H. Flores, D.P.B. Peixoto, L.G. Appel, R.R.D. Avillez, M.I.P.D. Silva, Catal. Today **172**, 218 (2011)
28. D. Varisli, G. T. Dogu, Dogu. Ind. Eng. Chem. Res **47**, 4071 (2008)
29. A.I. Osman, J.K. Abu-Dahrieh, D.W. Rooney, S.A. Halawy, M.A. Mohamed, A. Abdelkader, Appl. Catal. B **127**, 307 (2012)
30. T. Takeguchi, K.I. Yanagisawa, T. Inui, M. Inoue, Appl. Catal. A **192**, 201 (2000)
31. R.Z. Chu, X.Y. Wei, Z.M. Zong, W.J. Zhao, Front. Chem. Eng. China **4**, 452 (2010)
32. X.L. Meng, Y.F. Liu, Z.C. Zhang, R.Z. Chu, Z.M. Zong, X.Y. Wei, Appl. Mech. Mater. **66–68**, 1193 (2011)
33. Y. Tavan, M.R.K. Nikou, A. Shariati, J. Ind. Eng. Chem. **20**, 668 (2013)
34. P.B. Lihitkar, S. Violet, M. Shirolkar, J. Singh, O.N. Srivastava, R.H. Naik, S.K. Kulkarni, Mater. Chem. Phys. **133**, 850 (2012)
35. A.F. Hassan, S.A. Helmy, A. Donia, J. Braz, Chem. Soc. **26**, 1367 (2015)
36. M. Selvaraj, P.K. Sinha, A. Pandurangan, Microporous Mesoporous Mater. **70**, 81 (2004)
37. N.E. Poh, H. Nur, M.N.M. Muhid, H. Hamdan, Catal. Today **114**, 257 (2006)
38. F. Peng, L. Zhang, H. Wang, H.P. Lv Yu, Carbon **43**, 2405 (2005)
39. T.F. Parangi, R.M. Patel, U.V. Chudasama, Bull Mater. Sci. **37**, 609 (2014)
40. R. Sainath, K. Sangavi, S.S. Swain, D. Sangeetha, Int. J. Chem. Tech. Res. **7**, 3100 (2015)
41. X. Ma, S. Velu, J.H. Kim, C. Song, Appl. Catal. B **56**, 137 (2005)
42. E.E. Platero, M.P. Mentruit, Catal. Lett **30**, 31 (1994)
43. R.A. Mitran, D. Berger, L. Băjenaru, S. Năstase, C. Andronescu, C. Matei, Cent. Eur. J. Chem. **12**, 788 (2014)